Peptide Backbone Chemistry and Membrane Channel Function: Effects of a Single Amide-to-Ester Replacement on Gramicidin Channel Structure and Function†

Anthony R. Jude,‡ Lyndon L. Providence,§ Sigrid E. Schmutzer,‡ S. Shobana,§ Denise V. Greathouse,‡ Olaf S. Andersen,*,§ and Roger E. Koeppe II*,‡

Department of Chemistry and Biochemistry, University of Arkansas, Fayetteville, Arkansas 72701 and Department of Physiology and Biophysics, Weill Medical College of Cornell University, New York, New York 10021

Received July 6, 2000; Revised Manuscript Received November 2, 2000

ABSTRACT: To examine the structural and functional importance of backbone amide groups in ion channels for subunit folding, hydrogen bonding, ion solvation, and ion permeation, we replaced the peptide bond between Val^1 and Gly^2 in gramicidin A by an ester bond. The substitution is at the junction between the two channel subunits, where it removes an intramolecular hydrogen bond between the NH of Gly^2 and the C═O of Val^7 and perturbs an intermolecular hydrogen bond between the C═O of Val^1 in one subunit and the NH of Ala^5 in the other subunit. The substitution thus perturbs not only subunit folding but also dimer assembly, in addition to any effects on ion permeation. This backbone modification has large effects on channel function: It alters channel stability, as monitored by the channel forming ability and channel lifetime, and ion permeability, as monitored by changes in single-channel conductance and cation permeability ratios. In fact, the homodimeric channels, with two ester-containing subunits, have lifetimes so short that it becomes impossible to characterize them in any detail. The peptide → ester substitution, however, does not affect the basic subunit fold because heterodimeric channels can form between a subunit with an ester bond and a native subunit. These heterodimeric channels, with only a single ester bond, are more easily characterized; the lone ester reduces the single-channel conductance about 4-fold and the lifetime about 200-fold as compared to the native homodimeric channels. The altered channel function results from a perturbation/disruption of the hydrogen bond network that stabilizes the backbone, as well as the membrane-spanning dimer, and that forms the lining of the ion-conducting pore. Molecular dynamics simulations show the expected destabilization of the modified heterodimeric or homodimeric channels, but the changes in backbone structure and dynamics are remarkably small. The ester bond is somewhat unstable, which precluded further structural characterization. The lability also led to a hydrolysis product that terminates with an alcohol and lacks formyl-Val. Symmetric channels formed by the hydrolyzed product again have short lifetimes, but the channels are distinctly different from those formed by the ester gramicidin A. Furthermore, well-behaved asymmetric channels form between the hydrolysis product and reference subunits that have either an L- or a D-residue at the formyl-NH-terminus.

In protein chemistry, useful conceptual distinctions generally are made between the main chain and side chain atoms. While the variable side chains determine the folding of a protein within the context of a constant main-chain chemistry, it is nevertheless the backbone that dominates the structure. (In fact, popular computer programs for illustrating protein structures often depict backbone helices, sheets, and turns without side chains.) This main-chain scaffolding, with its characteristic secondary and tertiary structures, serves to organize side chain functional groups in geometries that are appropriate to support protein function. Protein structure−function studies therefore usually have probed how mutational changes of selected amino acid side chains affect function (and/or folding), within a framework where the backbone amide chemistry has been kept constant.

Recently, attention has been shifting toward backbone modifications, and several specific ester substitutions have been used to address the importance of backbone hydrogen bonding interactions for soluble globular protein structure and function. Wollmer and co-workers (*1*) incorporated a backbone ester into insulin to remove a structurally important hydrogen bond between the amide NH of Phe B25 and the carbonyl oxygen of Tyr A19. The resulting "depsi-insulin" structure was found to rearrange so as to bury Phe B25 into the protein's hydrophobic core (*2*). The contributions of several intramolecular backbone hydrogen bonds for α-helix stability and protein folding were investigated using specific backbone amide-to-ester substitutions in T4 lysozyme (*3*). In other studies (*4*, *5*), single backbone esters were used to assess the importance of intermolecular main chain hydrogen bonds for the recognition of serine proteases by their

† This work was supported in part by Grants GM34968 and GM21342 from the NIH. Anthony Jude's present address is Department of Chemistry, University of Arkansas at Little Rock, Little Rock, AR 72204.

* To whom correspondence should be addressed at the University of Arkansas, telephone: 501-575-4976; fax: 501-575-4049; e-mail: rk2@uark.edu; or at Weill Medical College, e-mail: sparre@med.cornell.edu.

‡ University of Arkansas.

§ Weill Medical College of Cornell University.

10.1021/bi001562y CCC: $20.00
Published on Web 01/11/2001

inhibitors. Similarly, binding experiments have been done using small thermolysin inhibitors (*6*) or vancomycin-binding peptides (*7*) with amide → ester replacements. Depsipeptide analogues of elastin repeating sequences have been synthesized (*8*), although these are relatively unstable.

Within a hydrophobic membrane environment (sequestered from water), the polar backbone moieties are likely to assume even greater functional importance. It therefore becomes important to investigate the significance of backbone chemistry and hydrogen bonding in integral membrane proteins. To this end, peptide → ester substitutions were introduced into the putative membrane-spanning α-helices of the nicotinic acetylcholine receptor (*9*). Even though the backbone substitutions (presumably) were far from the agonist binding site, they altered the concentrations for half-maximal activation by up to 20-fold, indicating that peptide → ester substitutions can exert significant effects on the conformational change from a closed to an open channel.

More generally, the structural importance of the (transmembrane) backbone is manifest in the substantial energetic cost for burying an unsatisfied hydrogen-bond "seeker" (donor or acceptor) within a lipid bilayer (*10*, *11*). The small yet growing set of crystal structures of transmembrane proteins shows an overwhelming preference (reviewed in ref *12*) for hydrogen-bonded backbone structures: usually α-helices (e.g., ref *13*), sometimes *β*-barrels (*14*). The peptide backbone groups, furthermore, may have direct functional roles, as suggested by the observation that the 12 Å long selectivity filter in the *KcsA* potassium channel is lined exclusively by main chain atoms (*15*). Indeed, the potassium channel structure suggests that backbone chemistry could be very significant for the function of ion-permeable channels (in particular for their ion selectivity).

Membrane-spanning ion channels catalyze transmembrane ion movement by forming the walls of water-filled, continuous pores through which the ions traverse the hydrophobic interior of the bilayer; if the pore is narrow enough, the permeating ions must be solvated by polar groups in the wall of the pore (*16*, *17*). In the case of gramicidin channels (*16*, *18*), it has long been recognized (*19*−*22*) that the pore wall is formed by the main chain atoms and that the amino acid side chains do not contact the permeating ions, which are (partially) solvated by the backbone carbonyl groups. This structural motif and permeation mechanism are not unique to gramicidin channels, as noted above, because the selectivity filter in the *KcsA* potassium channel also is lined by main chain atoms (*15*). The peptide backbone organization, however, differs between these channels. In gramicidin A (gA)[1] channels, the backbone is organized in a $\beta^{6.3}$-helix (where the carbonyl oxygens form hydrogen bonds with the amide hydrogens); in the *KcsA* channel the backbone is an extended peptide chain (where the carbonyl oxygens protrude into the channel lumen). The different organization means that the carbonyl oxygen/cation interactions and the details of ion solvation are likely to differ. The general similarity nevertheless raises an important question: how to evaluate the functional (and structural) importance of the peptide backbone, or any specific peptide carbonyl group, in a channel or other membrane-spanning protein?

In addition to effects on protein stability, the peptide backbone is likely to alter a protein's (an ion channel's) catalytic function directly, because the permeating ions are solvated by the backbone. We examined the role of the backbone for channel stability and ion permeation through a membrane-spanning channel following the lead of Eisenman (*23*) and replaced the O═C−NH between Val^1 and Gly^2 of gramicidin A by O═C−O. We designate this new depsi-peptide [Val-O-Gly]gA: HCO-Val^1-O-Gly^2-Ala-Leu-Ala-Val-Val^7-Val-Trp^9-Leu-Trp-Leu-Trp-Leu-Trp-$NHCH_2CH_2OH$, which has side chains identical to those of gA (the underlined residues are of D-chirality; selected residues, which will be discussed further, are numbered).

The peptide → ester substitution removes a stabilizing intramolecular hydrogen bond, between the NH of Gly^2 and the C═O of Val^7, and replaces it by a repulsive O ↔ O interaction, which will alter the energetics of subunit folding and assembly. The peptide → ester substitution also will alter the charge distribution in the C═O of Val^1 (*24*, *25*) and thus perturb the intermolecular hydrogen bond between the C═O of Val^1 in one subunit and the NH of Ala^5 in the other subunit, which will alter subunit association and dissociation. This charge redistribution further will weaken the interaction of the carbonyl oxygen with permeating cations (*26*) because the charge density on the carbonyl oxygen is reduced. [Val-O-Gly]gA does form channels, albeit with great difficulty. The structure of [Val-O-Gly]gA channels is similar to that of gA channels, but the functional characteristics of these channels differ dramatically from those of standard gramicidin A channels.

MATERIALS AND METHODS

Depsipeptide Synthesis and Purification. The dipeptide analogue f-Val-O-Gly was synthesized following Ono et al. (*27*): 2 mmol of formyl-L-valine (Bachem, King of Prussia, PA) and 2 mmol of benzyl-2-bromoacetate (Aldrich, Milwaukee, WI) were dissolved in dry benzene and refluxed while stirring in the presence of 1,8-diazobicyclo[5.4.0]-undec-7-ene (DBU, from Sigma Chemical Co., St. Louis, MO) for 2 hr under N_2. A DBU-HBr byproduct was removed by precipitation, by adding diethyl ether to the cooled reaction mixture. The desired formyl-L-Val-benzyl acetate was purified by extraction and chromatography over silica gel and was verified by ^{1}H NMR spectroscopy.

Dried formyl-L-Val-benzyl acetate was dissolved in ethyl acetate and catalytically hydrogenated over 5 wt % Pd on activated carbon (Aldrich) at 70 psi H_2 for 3 h, with continuous shaking. After extraction and drying, the dipeptide analogue, formyl-L-Val-glycolic acid (f-Val-O-Gly) was characterized by ^{1}H NMR spectroscopy in deuterated dimethyl sulfoxide: δ 8.50 ppm (d, J = 8.5 Hz, 1H), 8.09 (s, 1H), 4.61 (d, J = 15.8 Hz, 1H), 4.54 (d, J = 15.8 Hz, 1H), 4.38 (dd, J = 5.3 Hz, 8.7 Hz, 1H), 2.20−2.08 (m, 1H), 0.93 (d, J = 1.6 Hz, 3H), 0.90 (d, J = 1.6 Hz, 3H).

The susceptibility of f-Val-O-Gly to ester hydrolysis was tested in methanol solution at room temperature and was monitored by mass spectrometry. The peak corresponding to f-Val-O-Gly at m/z of 203 (expected 203.19) was converted slowly to a peak corresponding to f-Val-OH at m/z of 145 (expected 145.16). The half-time for the hydrolysis under these conditions was about 60 days. (The material was stable, with no detectable hydrolysis, at −20 °C.)

[1] Abbreviations: gA, gramicidin A; e, ethanolamine; f, formyl; MD, molecular dynamics; SDS, sodium dodecyl sulfate.

The depsi-gramicidin, [Val-O-Gly]gA, was synthesized by solid-phase methods (*28*) on a 0.02 mmol scale (3-mL reaction vessel) using a Trp-Sasrin-resin (Bachem) on an Applied Biosystems (Foster City, CA) 431A synthesizer. Fmoc-amino acid precursors were used for residues D-Leu^{14} through Ala^{3}, and the ester bond was introduced by the coupling of f-Val-O-Gly as the last step on the resin. The ester-containing gA analogue was removed from the resin with 10% ethanolamine (distilled, from Aldrich) in dimethylformamide at −10 °C (16 h). The final product was purified by reversed-phase chromatography using a 4.6 × 250 mm "Zorbax-C8" column of 5 μm octylsilica (MacMod Analytical, Chadds Ford, PA). The ester-containing gA analogue, [Val-O-Gly]gA, hydrolyzes readily at room temperature, thus precluding characterization using circular dichroism (CD) spectroscopy.

Electrophysiology. Single-channel measurements were as in Providence et al. (*29*) using bilayers of diphytanoylphosphatidylcholine (DPhPC)/*n*-decane, 1.0 M CsCl, and 200 mV transmembrane potential. The current traces were filtered at 500 Hz if a backbone ester was present or at 100 Hz for the nonester gramicidins. The single-channel experiments were done at 25 °C. To avoid hydrolysis, the depsi-peptide [Val-O-Gly]gA was stored in ice, and the experiments were conducted soon after (within a couple of hours) the addition of [Val-O-Gly]gA to the Teflon chamber.

Biionic potential measurements were done on bilayers separating a 1.0 M CsCl solution from a 1.0 M NaCl (or KCl) solution using an AxoPatch 1B (Axon Instruments, Foster City, CA) with the NaCl solution as the electrical reference. Bilayers were formed in the presence of a gramicidin concentration sufficiently high to ensure that the biionic potential (V_{bi}) was attained within a second, or so, after the bilayer formed. (The measured potentials were corrected for the liquid-junction potential between the two electrolyte solutions.) The permeability ratio (P_{Cs}/P_{Na}) was determined as $P_{Cs}/P_{Na} = \exp\{-V_{bi}F/(RT)\}$, where F is Faraday's constant, R the gas constant, and T the temperature in Kelvin. P_K/P_{Na} and P_{Cs}/P_K were determined similarly.

Molecular Dynamics (MD). MD simulations were done using CHARMM (*30*) academic version 24b2 using the PARAM23 all-atom force field (*31*). The simulations were carried out on three systems: a homodimeric gA channel, a homodimeric [Val-O-Gly]gA channel and a heterodimeric [Val-O-Gly]gA/gA channel. The calculations were done using a dielectric constant of 1 and three different assignments of the charge distribution at the ester bond: In all cases, the partial charge at the -O- was −0.34 e ($e = 1.602 \times 10^{-19}$ Coulomb), which should be compared with a partial charge at the NH group of −0.16 e; the charge difference was compensated at either the carbonyl C (0.51 $e \rightarrow$ 0.69 e), at Cα (−0.02 $e \rightarrow$ 0.16 e), or by splitting the difference between the two carbons. Each channel type was simulated in vacuo with 22 TIP3P (*32*) water molecules (10 H_2O in the single file region and six at each pore entrance, cf. ref *33*). The gA channel coordinates were derived from the Arseniev structure (*21*), and the hybrid and homodimeric [Val-O-Gly]gA channels were obtained by simple substitutions of N^2H to O^2. Following ref *33*, the H_2O molecules were subjected to a soft quadratic restoring potential, and the non-hydrogen atoms of the tryptophans were subjected to a weak harmonic restraint of 0.4 kJ/mol/Å^2. All atoms, including the hydrogens, were used in the calculation. The three channel structures were minimized energetically until the norm of the gradient was less than 0.004 kJ/mol/Å. MD studies then were done on the energy-minimized channels at 300 K using a time step of 0.2 fs and the SHAKE algorithm (*34*) to constrain the bonds involving hydrogens. Electrostatic interactions were calculated on a group-wise basis with no truncation (and the nonbonded cutoff distance set to 65 Å). First, the three channels were slowly heated (in 6 ps) to 300 K and equilibrated for 20 ps. The equilibrated channels were then used for production runs of 1 ns. The coordinate and velocity frames were stored at 0.1 ps intervals and the stored trajectories were used to compute the average structure and analyze fluctuations of geometric parameters and thermodynamic properties of the channel.

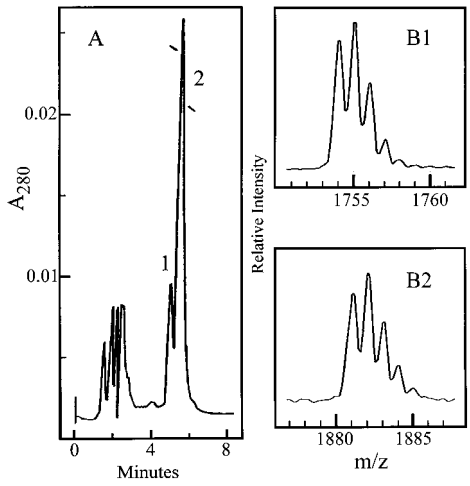

FIGURE 1: (A) HPLC trace of [Val-O-Gly]gA. Following the solvent signals, peaks 1 and 2 correspond to [HO-Gly]gA and [Val-O-Gly]gA, respectively. [Val-O-Gly]gA was collected from the top of peak 2 as indicated by the marks. (B) Negative-ion electrospray mass spectra from the components that were collected from peak 1 (B1) and peak 2 (B2). In panels B1 and B2, the families of peaks represent "M" minus H^+ with increasing numbers (0, 1, 2, 3, etc.) of naturally abundant ^{13}C atoms, where "M" is the monoisotopic (100% ^{12}C) molecular mass: 1755 for [HO-Gly]gA in B1, and 1882 for [Val-O-Gly]gA in B2. For reference, the monoisotopic mass of natural gA is 1881 (not shown). (During sample preparation and/or mass spectral analysis, some of peak 2 breaks down to yield peak 1, and so "M" of both 1755 and 1882 are routinely observed when peak 2 is analyzed.)

RESULTS

The depsi-gramicidin A was synthesized successfully but was somewhat labile even in neutral alcoholic solutions at 4 °C. During purification by HPLC, two peaks are seen (Figure 1, panel A) because [Val-O-Gly]gA undergoes moderately rapid hydrolytic cleavage to yield a 13-residue hydrolysis product, glycolyl-des-(formyl-valyl-glycyl)-gA, which we designate "[HO-Gly]gA," and whose sequence is given in Table 1. On the basis of electrospray mass spectrometry, the material in the first peak in the HPLC trace is [HO-Gly]gA (monoisotopic mass 1755; Figure 1, panel B1), and the material in the second peak is [Val-O-Gly]gA (monoisotopic mass 1882, i.e., 1 Da higher than gA; Figure 1, panel B2).

Channel Formation and Helix Sense. Both [Val-O-Gly]-gA and [HO-Gly]gA form channels in planar bilayers. The

Table 1: Sequences of Gramicidins Used in This Work[a]

Name	Length	Helix Sense	Sequence
[HO-Gly]gA	13+	RH	$HOCH_2C(O)$-A-L-A-V-V-V-W-L-W-L-W-L-W-e
des-Val-gA$^-$	14	LH	HCO-G-A-L-A-V-V-V-W-L-W-L-W-L-W-e
gA	15	RH	HCO-V^1-G-A-L-A-V-V-V-W-L-W-L-W-L-W^{15}-e
[Val-O-Gly]gA	15	RH	HCO-V*G-A-L-A-V-V-V-W-L-W-L-W-L-W-e
endo-D-Ala^{0a}-gA	16	RH	HCO-A-V-G-A-L-A-V-V-V-W-L-W-L-W-L-W-e
endo-Ala^{0a}-gA$^-$	16	LH	HCO-A-V-G-A-L-A-V-V-V-W-L-W-L-W-L-W-e
endo-Ala^{0a}-D-Ala^{0b}-gA	17	RH	HCO-A-A-V-G-A-L-A-V-V-V-W-L-W-L-W-L-W-e

[a] The one-letter amino acid code is used. D-Residues are underlined. The end blocking groups are -e, ethanolamide; HCO-, formyl; and $HOCH_2C(O)$-, glycolyl. The ester bond in [Val-O-Gly]gA is indicated by an asterisk (*).

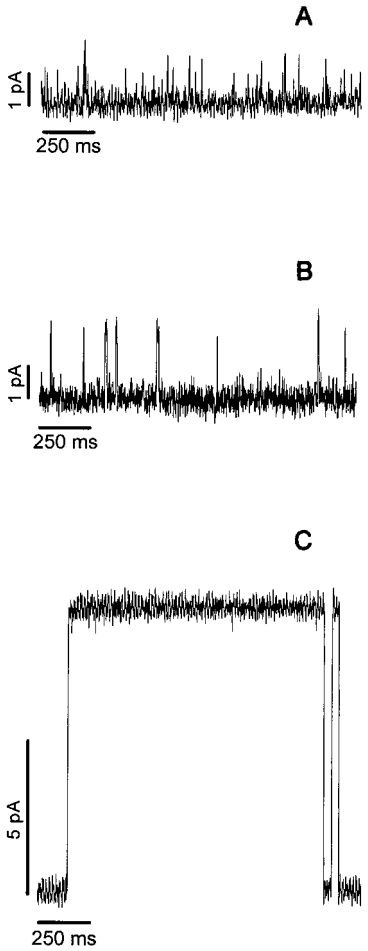

FIGURE 2: Single-channel current traces obtained after symmetric addition of [Val-O-Gly]gA (A), [HO-Gly]gA (B), and gA (C). DPhPC/*n*-decane bilayers, 1.0 M CsCl, 200 mV, 500 Hz.

properties of the channels formed by either compound differ markedly from those of gA channels (Figure 2). In 1.0 M CsCl (200 mV), the [Val-O-Gly]gA channels (Figure 2, panel A) have lifetimes <1 ms (or ~1000-fold less than gA channels); their predominant single-channel current transitions are ~1 pA (or 10-fold less than for gA channels), but the transitions are poorly resolved and the actual current amplitudes are higher than they appear in the traces. The [HO-Gly]gA channels (Figure 2, panel B) have longer lifetimes and the channel events can be resolved; their average lifetime is ~4 ms and the predominant single-channel current transitions are ~2 pA (histograms not shown). In addition to the reduced lifetime, the channel-forming propensities of [Val-O-Gly]gA or [HO-Gly]gA are reduced: we need to add ~10-fold more of either analogue than of gA to obtain comparable channel appearance rates (~1/s).

For either [Val-O-Gly]gA or [HO-Gly]gA, the channel appearance rate is >100-fold higher when the compound is added to both sides of a bilayer, as compared to when it is added to only one side (cf. Figure 2, and Figures 3−5, below), indicating that the channels are single-stranded dimers of $\beta^{6.3}$-helices (*35*, *36*). To further verify that the channels formed by the addition of either [Val-O-Gly]gA or [HO-Gly]gA are different entities, and to determine their global fold, we used heterodimer formation experiments (*37*, *38*) with gA, its mirror-image gA$^-$, and the sequence-extended analogues *endo*-D-Ala^{0a}-gA, *endo*-Ala^{0a}-D-Ala^{0b}-gA, and *endo*-Ala^{0a}-gA$^-$, as well as the sequence-shortened des-Val-gA$^-$ as reference compounds (Table 1). The reference gA analogues form right-handed channels, whereas the gA$^-$ analogues form left-handed channels (*36*, *38*, *39*). The hydrogen bond-stabilized junction between the two subunits in a membrane-spanning channel requires that both subunits have the same helix sense (*29*, *39*); heterodimer formation thus becomes a sensitive method to determine changes in handedness, or more generally to ascertain whether the channel structure has been significantly affected by a sequence modification. (It was necessary to use reference analogues with both even and odd numbers of residues, because the alternating L−D sequence will leave a gap at the junction between two different monomers unless their formyl-NH-terminal residues have the same chirality (*36*, *38*).)

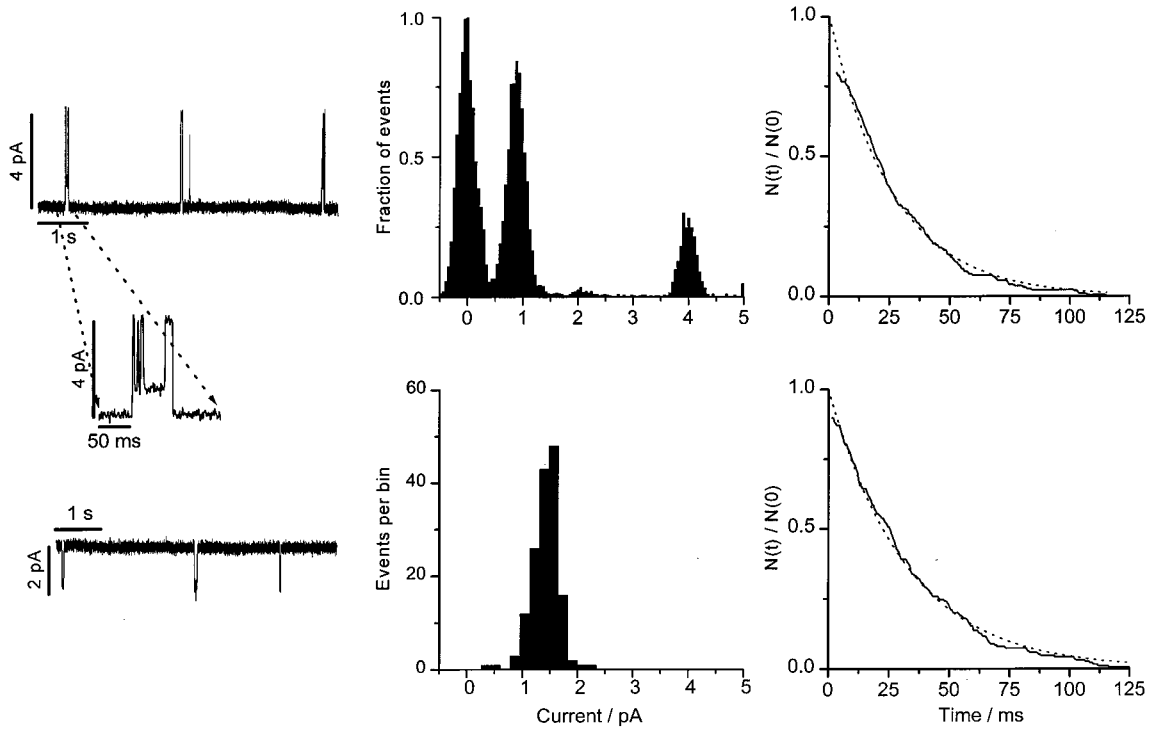

FIGURE 3: Single-channel current traces (left), current amplitude histograms (middle) and lifetime histograms (right) observed when [Val-O-Gly]gA and *endo*-Ala^{0a}-D-Ala^{0b}-gA each is added to only one side of a bilayer. The top row shows results when the [Val-O-Gly]gA subunit is facing the positive solution; the lower row shows results when the [Val-O-Gly]gA subunit is facing the negative solution. At either polarity, there is one distinct channel type, but the single-channel appearances differ markedly at the two polarities. At +200 mV, when the current is in the [Val-O-Gly]gA → *endo*-Ala^{0a}-D-Ala^{0b}-gA direction, the channel appearances show two-state behavior with a low-conductance ($i \approx 0.9$ pA) and a high-conductance ($i \approx 4$ pA) state (shown in more detail in the expanded current trace), as also is evident in the current-level histogram (based on 152 individual channel appearances, for which the ordinate denotes the fraction of time the current is at the indicated level, normalized to the maximal value at 0 pA). Despite the complexity of the channel appearances, the lifetime distribution is described by a single-exponential distribution with $\tau = 26$ ms. At −200 mV, there is a single well-defined current amplitude with $i = 1.5 \pm 0.2$ pA and $\tau = 32$ ms ($n = 121$). DPhPC/*n*-decane, 1.0 M CsCl, 500 Hz.

The LH gA$^-$ reference analogues do not form heterodimers with either [Val-O-Gly]gA or [HO-Gly]gA (results not shown), meaning that the latter two compounds do not form left-handed $\beta^{6.3}$-helices. The RH gA analogues, however, do form heterodimers with [Val-O-Gly]gA as well as with [HO-Gly]gA and, for a given gA analogue, the respective heterodimers are quite distinct (Figures 3−5, below). Moreover, when a sample of [Val-O-Gly]gA is allowed to sit at 25 °C for a week, the heterodimer appearances shift to those observed with [HO-Gly]gA (results not shown). We conclude that [Val-O-Gly]gA and [HO-Gly]gA form unique conducting channels and that these channels are dimers of right-handed $\beta^{6.3}$-helices. (The [Val-O-Gly]gA/gA heterodimers had lifetimes that were so brief that we limit the presentation of the experimental results to those obtained using *endo*-D-Ala^{0a}-gA and *endo*-Ala^{0a}-D-Ala^{0b}-gA as reference subunits.)

Bistable Channels. Figure 3 shows the results of heterodimer channel formation experiments between [Val-O-Gly]-gA and a reference 17-residue subunit of *endo*-Ala^{0a}-D-Ala^{0b}-gA, which is held constant throughout the heterodimer experiments (Figures 3−5). The experiments were done using an "asymmetric protocol", in which the reference compound is added to one side of the bilayer and the "test" gramicidin is added to the other side. In these experiments, the heterodimers are oriented in the bilayer because the monomers tend to be anchored to the aqueous solution to which they were added (*35*). One thus can distinguish channels in which the current flow is from the [Val-O-Gly]gA to the *endo*-Ala^{0a}-D-Ala^{0b}-gA subunit (when the [Val-O-Gly]gA-containing electrolyte solution is positive relative to the *endo*-Ala^{0a}-D-Ala^{0b}-gA-containing electrolyte solution) from those in which the current flow is reversed. (In this and the following experiments, the *endo*-Ala^{0a}-D-Ala^{0b}-gA-containing electrolyte solution will be the electrical reference.)

When [Val-O-Gly]gA is added to one side of a bilayer and *endo*-Ala^{0a}-D-Ala^{0b}-gA is added to the other side, we see a single predominant channel type, which is a [Val-O-Gly]gA/*endo*-Ala^{0a}-D-Ala^{0b}-gA heterodimer (Figure 3). There is, however, marked asymmetry in the pattern of channel appearances as a function of the applied potential. At negative potentials, when the current is in the *endo*-Ala^{0a}-D-Ala^{0b}-gA → [Val-O-Gly]gA direction, the channel appearances are "regular" with a current transition amplitude of ∼1.5 pA. By contrast, at positive potentials, when the current is in the [Val-O-Gly]gA → *endo*-Ala^{0a}-D-Ala^{0b}-gA direction, the channel appearances exhibit rapid transitions between two current levels at ∼1 and ∼4 pA. Such a pattern of multiple conductance levels indicates that the channels are bistable, i.e., they have at least two different conformations that conduct cations. Similar results have been seen with some other heterodimeric gramicidin channels, for example, *endo*-Gly^{0a}-gA/gA (*38*) and [F$_6$Val^1]gA/gA (*40*). In all cases, the bistable channel behavior correlates with a steric perturbation at the junction between the gramicidin subunits.

Despite the asymmetry in the pattern of [Val-O-Gly]gA/*endo*-Ala^{0a}-D-Ala^{0b}-gA channel appearances, there is little asymmetry in the heterodimer lifetime distributions with respect to the applied potential (Figure 3).

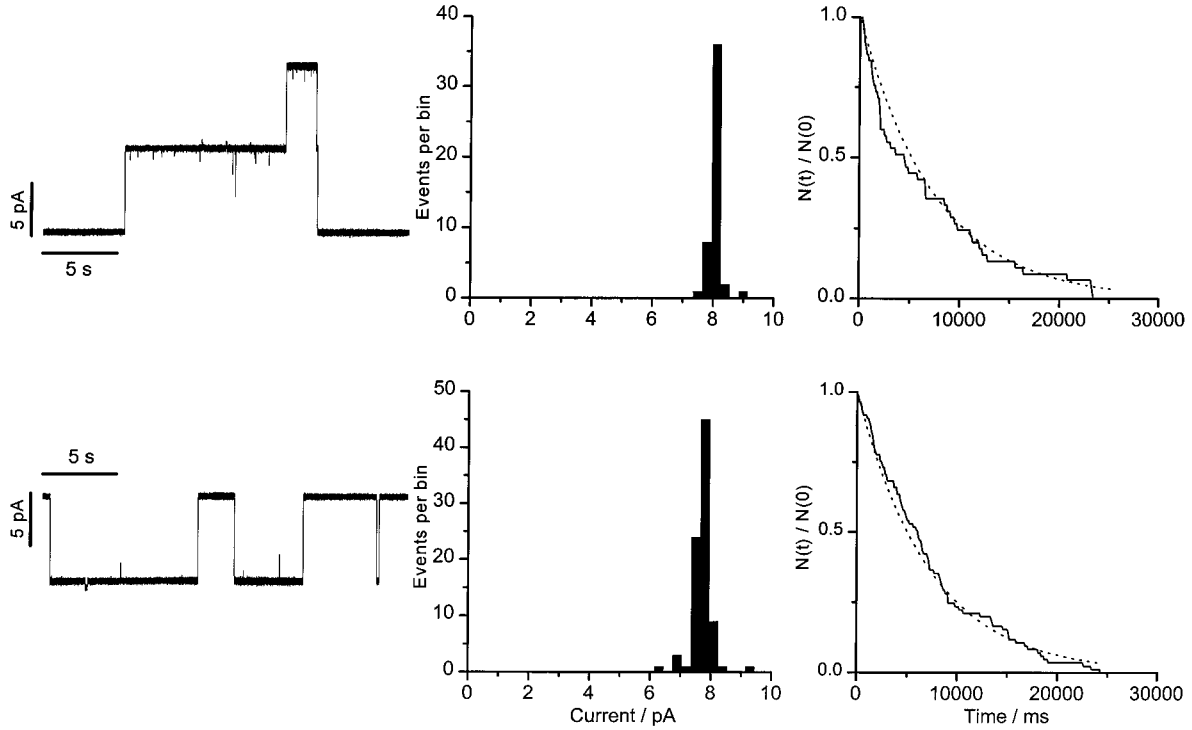

FIGURE 4: Single-channel current traces (left), current amplitude histograms (middle), and lifetime histograms (right) observed when gA and *endo*-Ala^{0a}-D-Ala^{0b}-gA each is added to only one side of a bilayer. The top row shows results when the gA subunit is facing the positive solution; the lower row shows results when the gA subunit is facing the negative solution. At either polarity, there is one distinct channel type. At +200 mV, when the current is in the gA → *endo*-Ala^{0a}-D-Ala^{0b}-gA direction, the average single-channel current (*i*) is 8.0 ± 0.1 pA and τ = 7.5 s (n = 49). At −200 mV, i = 8.0 ± 0.2 pA, and τ = 7.2 s (n = 85). DPhPC/*n*-decane, 1.0 M CsCl, 500 Hz.

For comparison, Figure 4 illustrates the properties of heterodimeric channels formed between native gA and *endo*-Ala^{0a}-D-Ala^{0b}-gA. These hybrid channels differ from those of Figure 3 only by the absence of the ester substitution in the backbone of the 15-residue subunit (with the *endo*-Ala^{0a}-D-Ala^{0b}-gA subunit being constant). In this case, there is little asymmetry in the channel appearances: the current transition histograms are indistinguishable for the two heterodimer orientations, as are the average lifetimes.

Channel Activity with a Hydrolyzed Subunit. In the case of [HO-Gly]gA/*endo*-Ala^{0a}-D-Ala^{0b}-gA heterodimers (Figure 5), there is little asymmetry in the channel appearance pattern at the two polarities, and the current transition amplitude and lifetime distributions are similar for the two heterodimer orientations.

The [Val-O-Gly]gA/*endo*-Ala^{0a}-D-Ala^{0b}-gA and [HO-Gly]gA/*endo*-Ala^{0a}-D-Ala^{0b}-gA heterodimers differ not only in terms of the channel appearances and asymmetry: the [HO-Gly]gA/*endo*-Ala^{0a}-D-Ala^{0b}-gA heterodimers have an average lifetime that is 20-fold longer than that of [Val-O-Gly]gA/*endo*-Ala^{0a}-D-Ala^{0b}-gA heterodimers. This result is surprising because [HO-Gly]gA/*endo*-Ala^{0a}-D-Ala^{0b}-gA channels would be expected to have a partial mismatch at the junction between the monomers: a 17-residue subunit that has a (proper) formyl terminal opposite a 13-residue subunit that has a (variant) glycolyl terminal.[2]

To better understand the basis for the [HO-Gly]gA/*endo*-Ala^{0a}-D-Ala^{0b}-gA heterodimer stability, we examined the heterodimers formed between [HO-gA]gA and the 16-amino acid analogue *endo*-D-Ala^{0a}-gA (Figure 6). Because the reference analogue has a D-residue at the formyl-NH-terminus, these heterodimers should have similar length as the [HO-Gly]gA/*endo*-Ala^{0a}-D-Ala^{0b}-gA heterodimers, but the [HO-Gly]gA/*endo*-D-Ala^{0a}-gA heterodimers would be expected to be relatively destabilized because a one-residue mismatch at the subunit junction should cause a substantial decrease in channel lifetime relative to gA homodimers (*38*). Indeed, the [HO-Gly]gA/*endo*-D-Ala^{0a}-gA heterodimers have shorter lifetimes than the [HO-Gly]gA/*endo*-Ala^{0a}-D-Ala^{0b}-gA heterodimers. Furthermore, the channel properties now vary depending on the polarity of the applied potential (Figure 6): at positive potentials, when the current is in the [HO-Gly]gA → *endo*-D-Ala^{0a}-gA direction, the channels have a lower conductance and a longer lifetime than at negative potentials. This asymmetry, taken together with the symmetric characteristics of the [HO-Gly]gA/*endo*-Ala^{0a}-D-Ala^{0b}-gA heterodimers (see Figure 5), shows that [HO-Gly]gA indeed should be considered to be a 13-amino acid analogue with a glycolyl-NH-terminus.

Cation Selectivity of Ester-Containing Channels. As a further test of the functional influence of the backbone ester, the ion selectivity of [Val-O-Gly]gA (homodimeric) channels was determined in biionic potential measurements (Cs^+/Na^+, K^+/Na^+, and Cs^+/K^+), using many-channel experiments. As compared to standard gA channels, [Val-O-Gly]gA channels

[2] To form dimeric membrane-spanning channels between two gramicidin monomers that have the same helix sense but differ in length by n residues, then n must be zero or even to have a smooth subunit junction. If n is odd, the heterodimeric channels will miss a residue near the center of the bilayer, which means that they are destabilized by about 10 kJ/mol relative to the symmetric parent channels (*38*). Therefore, a 17-residue subunit should be compatible with a 13-residue subunit, but the extra atoms in the $HOCH_2CO$ terminal of [HO-Gly]gA would destabilize the resulting channels relative to those with the usual HCO.

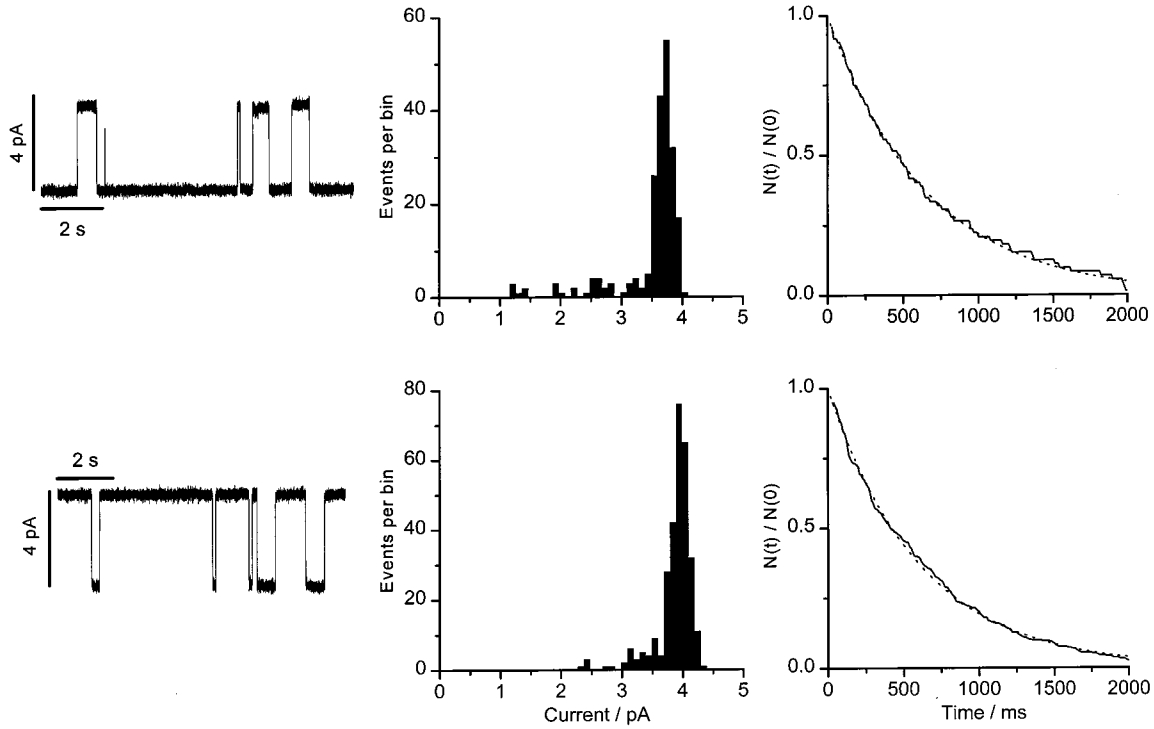

FIGURE 5: Single-channel current traces (left), current transition amplitude histograms (middle), and lifetime histograms (right) observed when [HO-Gly]gA and *endo*-Ala^{0a}-D-Ala^{0b}-gA each is added to only one side of a bilayer. The top row shows results when the [HO-Gly]gA subunit is facing the positive solution; the lower row shows results when the [HO-Gly]gA subunit is facing the negative solution. At either polarity, there is one distinct channel type. At +200 mV, when the current is in the [HO-Gly]gA → *endo*-Ala^{0a}-D-Ala^{0b}-gA direction, the average single-channel current $i = 3.7 \pm 0.1$ pA (mean ± SD) and $\tau = 660$ ms ($n = 71$); at −200 mV, $i = 4.0 \pm 0.1$ pA and $\tau = 610$ ms ($n = 331$). DPhPC/*n*-decane, 1.0 M CsCl, 500 Hz.

have reduced ion selectivity (Table 3). Surprisingly, both P_{Cs}/P_{Na} and P_{Cs}/P_K are less than 1.0, meaning that Cs^+ is (slightly) less permeant than K^+ or Na^+. This result is difficult to rationalize within the framework of a model that considers only ion solvation by the polar groups in the pore wall (see Discussion). A possible explanation is provided by the [Val-O-Gly]gA heterodimer results (Figure 3). The bistable behavior may suggest that the peptide → ester substitution causes a (subtle) change in the backbone structure, which in turn could reduce the Cs^+ permeability by reducing the pore radius.

Molecular Dynamics Simulations. In an attempt to get insight into why the peptide → ester substitution caused such a dramatic destabilization of the membrane-spanning channel, we performed MD simulations on three different gramicidin dimers: a gA/gA homodimer, a [Val-O-Gly]gA/[Val-O-Gly]gA homodimer, and a [Val-O-Gly]gA/gA heterodimer. As we were interested in structural perturbations at the subunit interface, the simulations were done in vacuo with the bilayer being represented by harmonic constraints. The conformational energies were determined every 100 ps during a 1-ns simulation. There was no systematic drift during the 1-ns simulation (the systems were well equilibrated at the beginning of the production runs), and the energies from the different 100 ps windows were averaged. The results were similar for all three choices of charge compensation; the results for full Cα compensation are summarized in Table 4 and described further below. As expected, the gA/gA homodimer has the lowest energy, the [Val-O-Gly]gA/[Val-O-Gly]gA homodimer has the highest energy (about 58 kJ/mol higher), and the [Val-O-Gly]gA/gA heterodimer is intermediate (with an energy about 16 kJ/mol higher than the gA/gA homodimer). The energy difference of ∼42 kJ/mol between the ester-containing heterodimer and the (disubstituted) homodimer is in reasonable agreement with what was expected from the experimental results (see Discussion). The major contributor to the energy differences is the electrostatic energy (up to ∼50 kJ/mol); all other energies are similar among the three dimers.

When the dimer structures are examined in detail, however, the conformational differences between the gA and the [Val-O-Gly]gA subunits are surprisingly small (Figure 7). (Figure 7 shows results obtained with the [Val-O-Gly]gA/gA heterodimer; the results for each monomer in the corresponding homodimers were indistinguishable from those shown here.)

The major difference between the monomers is in the average ω value for the Val-Gly (or Val-O-Gly) bond (left two panels), which differs by 8° (175° in gA vs 167° in [Val-O-Gly]gA) and in the larger dispersion of 10.5° for the standard deviation of ω in [Val-O-Gly]gA as compared to 8.2° in gA. When comparing the respective ω distributions for the first 100 ps and the last 100 ps simulations, there was no drift, meaning that the system was well equilibrated. Associated with this change in ω, the distance between ester O^2 and carbonyl O^7 was ∼0.25 Å longer (4.20 vs 3.95 Å) than the distance between amide N^2 and carbonyl O^7. Again, there was no systematic drift.

There also are small differences in the distributions of the coordinates for the carbonyl oxygens at positions 1 and 2 (for clarity only results for residues formyl 0 through 8 are shown in the center panels in Figure 7). The most notable difference is that carbonyl oxygen 2 in [Val-O-Gly]gA is "forced" farther out than it is in gA. More detailed examina-

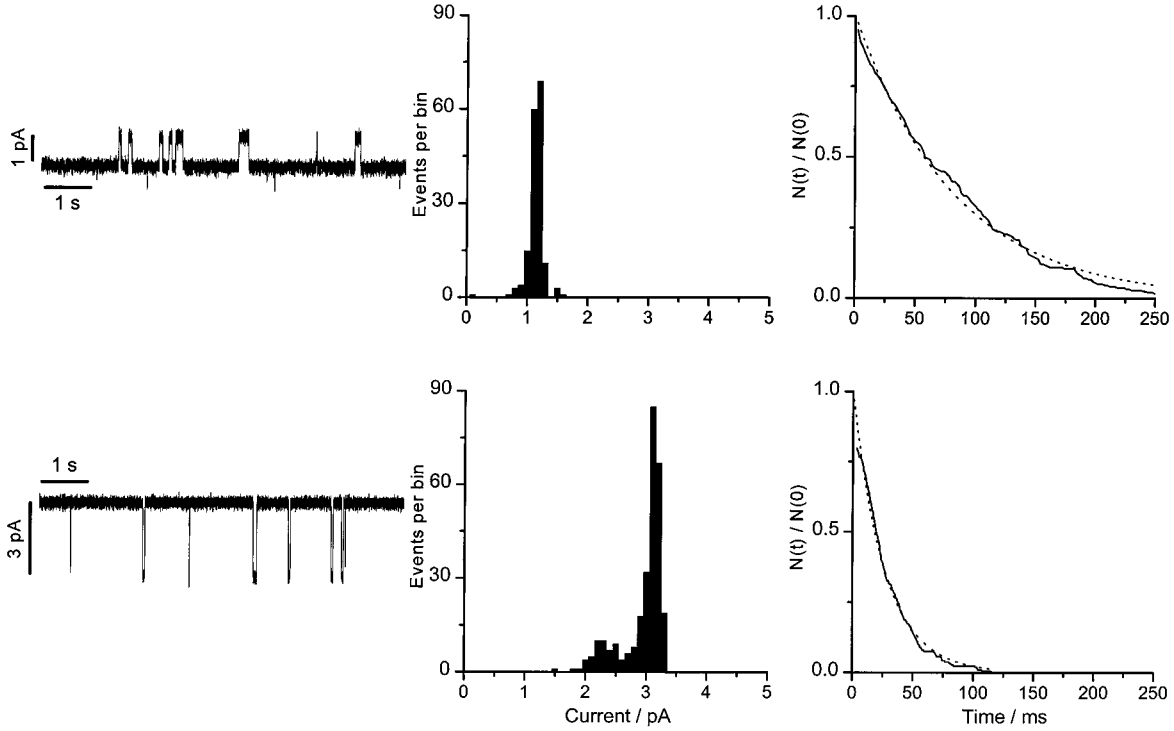

FIGURE 6: Single-channel current traces (left), current transition amplitude histograms (middle), and lifetime histograms (right) observed when [HO-Gly]gA and *endo*-D-Ala^{0a}-gA each is added to only one side of a bilayer. The top row shows results when the [HO-Gly]gA subunit is facing the positive solution; the lower row shows results when the [HO-Gly]gA subunit is facing the negative solution. At either polarity, there is one distinct channel type, but the single-channel current and lifetime vary with the applied potential. At +200 mV, when the current is in the [HO-Gly]gA → *endo*-D-Ala^{0a}-gA direction, the average single-channel current $i = 1.2 \pm 0.1$ pA (mean ± SD) and $\tau = 82$ ms ($n = 167$); at −200 mV, $i = 3.1 \pm 0.1$ pA and $\tau = 26$ ms ($n = 287$). DPhPC/*n*-decane, 1.0 M CsCl, 500 Hz.

Table 2: Summary of Conductance and Lifetime Results[a]

analogue	g (pS)	τ (ms)
Homodimers		
gA	50	500
endo-D-Ala^{0a}-gA	40	11 000
endo-Ala^{0a}-D-Ala^{0b}-gA	28	300 000
[Val-O-Gly]gA	<5	<1
[HO-Gly]gA	10	4
Heterodimers		
[Val-O-Gly]gA/*endo*-Ala^{0a}-D-Ala^{0b}-gA	20, 5 (+200 mV)	26
	8 (−200 mV)	32
gA/*endo*-Ala^{0a}-D-Ala^{0b}-gA	40 (+200 mV)	7500
	40 (−200 mV)	7200
[HO-Gly]gA/*endo*-Ala^{0a}-D-Ala^{0b}-gA	19	630
[HO-Gly]gA/*endo*-D-Ala^{0a}-gA	6 (+200 mV)	82
	16 (−200 mV)	26

[a] *g* is the single-channel conductance and τ is the lifetime in the presence of 1.0 M CsCl, ±200 mV. The polarity is noted when the results at +200 mV differ from those at −200 mV.

Table 3: Biionic Potentials and Permeability Ratios

gramicidin analogue	ion pair	biionic potential (mV)	permeability ratio
gA	Cs^+/Na^+	-31.6 ± 0.5	3.43 ± 0.06
	K^+/Na^+	-25.7 ± 0.2	2.73 ± 0.02
	Cs^+/K^+	-5.6 ± 0.3	1.24 ± 0.02
[Val-O-Gly]gA	Cs^+/Na^+	$+4.7 \pm 0.9$	0.83 ± 0.04
	K^+/Na^+	-8.0 ± 0.2	1.37 ± 0.02
	Cs^+/K^+	$+7.1 \pm 0.5$	0.76 ± 0.02

tion reveals that the trajectories for residues 0 and 1 also are shifted slightly. As an aside, the dispersion in the carbonyl positions in either subunit is much larger for residues 0 through 5, which are the residues at the subunit/subunit

Table 4: Results of Molecular Dynamics Simulations

dimer type	total energy[a]	major energy contributions: bond	angle	dihedral	van der Waals	electrostatic
gA/gA	−476.2	+91.0	+186.6	+495.2	−374.4	−907.1
	(16.7)	(1.3)	(1.1)	(10.0)	(8.7)	(19.7)
[Val-O-Gly]gA/	−418.0	+88.8	+186.5	+497.1	−369.7	−854.0
[Val-O-Gly]gA	(23.6)	(0.7)	(1.6)	(7.1)	(11.2)	(23.2)
[Val-O-Gly]gA/gA	−460.0	+88.6	+187.6	+490.2	−375.5	−884.9
	(22.1)	(1.2)	(4.0)	(8.9)	(14.8)	(30.7)

[a] Energies are in kJ/mol, with standard deviations in parentheses.

interface, than for residues 6−8, each of which participates in two intramolecular hydrogen bonds. (The dispersion increases again in residues 10−15; results not shown). The latter result confirms our initial conjecture that peptide → ester replacements close to the formyl-NH-terminus should be particularly sensitive to the structural perturbation induced by the replacement. Finally, one might expect that the correlated distribution of the positions for N^2 vs carbonyl O^7 would differ from the distribution of ester O^2 vs carbonyl O^7. The difference is surprisingly small; furthermore (right two panels), the distribution of O^2 vs carbonyl O^7 is relatively restricted as compared to that of N^2 vs carbonyl O^7.

The H···O distances for backbone hydrogen bonds in the gA/gA and [Val-O-Gly]gA/[Val-O-Gly]gA homodimers were calculated every 0.1 ps during the 1 ns simulation, and the distributions were analyzed. For gA/gA, the distances varied within a narrow range, the average distance being 1.885 ± 0.077 Å (mean ± standard deviation, $n = 30$) with a range of 1.71 to 2.03 Å. The average width of the distribution for a gA/gA backbone hydrogen bond, deter-

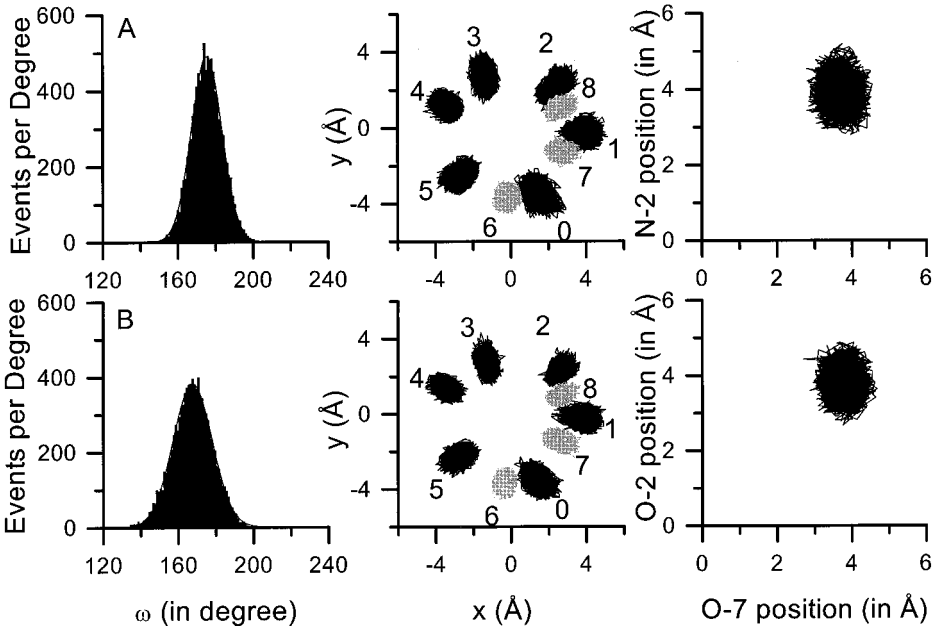

FIGURE 7: Results of molecular dynamic simulations for gA (A) and [Val-O-Gly]gA (B). The left two panels show the distribution of the ω dihedral angles: ($Cl^{\alpha}-C1-N2-C$) in gA (top) and ($C1^{\alpha}-C1-O2-C$) in [Val-O-Gly]gA (bottom). [The indices 1 and 2 refer to the first (Val) and second (Gly) residues.] The two center panels show the projection in the x−y plane of carbonyl oxygen positions of the first eight residues in gA (top) and [Val-O-Gly]gA (bottom). The residue numbered 0 denotes the formyl group at the amino terminus. Residues 6−8 participate solely in intramolecular hydrogen bonds (results shaded lighter gray), whereas the initial sequence of residues 0−5 participates in both intra- and intermolecular hydrogen bonds. [Specifically, residues 1, 3, and 5 make the intermolecular hydrogen-bond (dimerization) contacts.] The right two panels show the cross-correlation between the positions of carbonyl oxygen-7 and the amide N2 in gA (top) or the ester O2 in [Val-O-Gly]gA (bottom).

mined as the width at half-maximal height, was 0.353 ± 0.068, with a range from 0.26 to 0.51 Å. For the [Val-O-Gly]gA/[Val-O-Gly]gA homodimer, the average H···O distance was 1.893 ± 0.112 Å ($n = 24$), with a range of 1.73 to 2.25 Å, and the average width at half-maximal height was 0.368 ± 0.112 Å, with a range of 0.20 to 0.78 Å. The increased standard deviations and ranges arose from just two hydrogen bonds, in one of the [Val-O-Gly]gA subunits, that were longer than 2.03 Å: those between NH^6 and CO^{11} (length 2.13 Å, half-maximal width 0.61 Å) and NH^8 and CO^{13} (length 2.25 Å, half-maximal width 0.78 Å). The corresponding hydrogen bonds in the other [Val-O-Gly]gA subunit fell with the limits expected from the gA/gA homodimer. The two perturbed hydrogen bonds are on the same side of the monomers as the $O^2 \leftrightarrow CO^7$ contact. That is, even though the overall structure varies little between the gA/gA and the [Val-O-Gly]gA/[Val-O-Gly]gA homodimers, there is some propagated perturbation (and asymmetry) of the backbone structure.

In CHARMM, the hydrogen bond energy contributions are incorporated in the electrostatic (and van der Waals) energies. The peptide → ester substitution had little effect on the van der Waals energy but a major effect on the electrostatic energy (Table 4). We therefore focused on the electrostatic contribution. Using the CHARMM charges (see Materials and Methods) and the distances from the MD calculations, the electrostatic interaction energy between NH^2 and OC^7 (intramolecular) or between CO^1 and HN^5 (intermolecular) is about −10 kJ/mol. The corresponding electrostatic interaction energy between O^2 and OC^7 is about +20 kJ/mol, and there is little change in the intermolecular $CO^1 \cdots HN^5$ energy. That is, the overall energy difference between the [Val-O-Gly]gA/[Val-O-Gly]gA and the gA/gA dimer is similar to the difference in the electrostatic interaction energy between O^2 and OC^7 relative to NH^2 and OC^7.

Figure 7 is representative of a number of structural correlations that show little difference between gA and [Val-O-Gly]gA. Overall, the MD simulations indicate that the large changes in function induced by the peptide → ester substitution are due to energetic changes that result from (surprisingly small) changes in the channel's average structure and dynamics.

DISCUSSION

The goal of this study was to characterize gramicidin channels that have an ester substitution in the peptide backbone. The peptide → ester substitution should have minimal effects on the backbone stereochemistry, e.g., see ref *8*, but it will introduce two changes into the channel: first, the ester will alter the distribution of charges on the atoms involved in the covalent bond between the residues in question; and second, in the case of buried peptide groups, the ester will remove a stabilizing hydrogen bond and replace it by repulsive O ↔ O interactions. We chose to replace the normal Val−Gly bond by a Val-O-Gly bond for two reasons. First, the chemistry was feasible. Second, we surmised that a peptide → ester substitution at this position would be particularly sensitive to the structural perturbations that might be introduced by the substitution, and any strain at the subunit interface could be determined in appropriate heterodimer formation experiments (cf. refs *37* and *38*).

We found that when both subunits of a channel have the ester bond (see model in Figure 8), the channel events are very brief and difficult/impossible to analyze quantitatively. Furthermore, the chemical lability of the analogue precluded detailed characterization using conventional methods. To

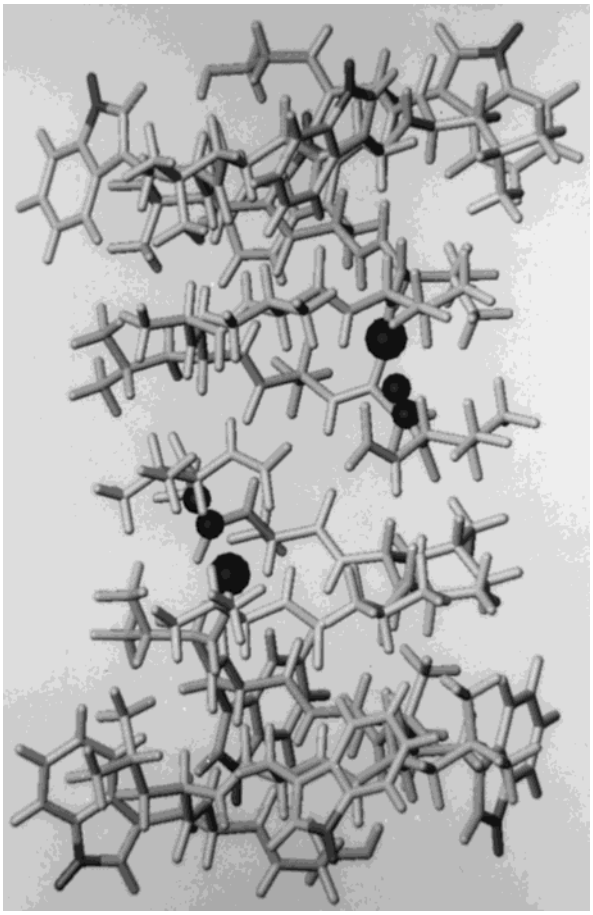

FIGURE 8: A stick model to show the locations at which an ester oxygen will replace the NH of Gly^2 in each subunit of a (homodimeric) gramicidin channel. The two pairs of smaller black spheres represent the NH groups that are to be replaced by oxygens. Each substitution will interrupt the hydrogen bond to the Val^7 C═O (larger black spheres, upper right and lower left) and will introduce an O ↔ O repulsion that interferes with proper folding of the first turn each monomer. The coordinates are from Arseniev et al. (*21*), as refined in ref *51*.

characterize channels with a peptide → ester substitution, it thus became necessary to focus on heterodimers formed between [Val-O-Gly]gA and a longer 17-residue (nonester) subunit, *endo*-Ala^{0a}-D-Ala^{0b}-gA. The resulting channels have a single backbone ester bond in only one subunit and therefore were more easily characterized. As compared to the reference gA/*endo*-Ala^{0a}-D-Ala^{0b}-gA heterodimers, the lifetime of the depsi-peptide channels was reduced some 200-fold and the conductance was reduced 2−3-fold. Most importantly, however, the fact that heterodimeric channels could be observed shows that [Val-O-Gly]gA can fold into a $\beta^{6.3}$-helix, even though the bi-stable channel behavior (Figure 3) indicates a stress at the [Val-O-Gly]gA/gA interface.

Channel Lifetime and Stability. The large reduction in the single-channel lifetime, together with the reduced channel-forming potency (of [Val-O-Gly]gA) suggests that the peptide → ester substitution causes a dramatic destabilization of the channel, most likely by introducing a "stress" in the depsi-peptide monomer. A disruption of the monomer backbone structure (Figure 8) in turn would hamper the docking of a second monomer. The MD simulations indicate an average energetic cost of ∼29 kJ/mol per ester containing subunit. (The estimated cost is about 16 kJ/mol for the first ester bond and about 42 kJ/mol for the second ester bond in a dimer; see Table 4. The asymmetry in the calculated results could suggest that a nonester subunit can adapt to an ester-containing partner.)

It is possible to compare the MD estimates to experimental estimates for these energy differences by noting that gramicidin channels form by a (transmembrane) dimerization reaction:

$$2\mathrm{M} \underset{k_d}{\overset{k_a}{\rightleftharpoons}} \mathrm{D}$$

where M denotes a nonconducting monomer, D the conducting dimer, and k_a and k_d the association and dissociation rate constants, respectively. The changes in k_d that result from the peptide → ester substitution can be determined from the channel lifetime: $k_d = \tau^{-1}$. τ is reduced about 1000-fold for the [Val-O-Gly]gA/[Val-O-Gly]gA channels, as compared to the gA/gA channels, so k_d is increased by a factor 10^3. The corresponding changes in k_a can be estimated by noting that the channel formation rate is given by $k_a[M]^2$ and that the experiments were done such that the channel appearance rates were comparable for the different channel types, which was achieved by varying the amount of each particular gramicidin that was added to each side of the bilayer. We need to add 10-fold more [Val-O-Gly]gA than gA to observe comparable appearance rates, which means that k_d is reduced by a factor 100. Altogether, these order of magnitude estimates lead to the conclusion that the dimerization constant, K (= k_a/k_d), for [Val-O-Gly]gA/[Val-O-Gly]gA channels is about 10^5-fold less than for gA/gA channels. That is, [Val-O-Gly]gA/[Val-O-Gly]gA dimers are destabilized by about 30 kJ/mol as compared to gA/gA dimers (in quite good agreement with the estimate of 58 kJ/mol from the MD simulations; Table 4).

The asymmetric current−voltage behavior and decreased lifetime of the [Val-O-Gly]gA/*endo*-Ala^{0a}-D-Ala^{0b}-gA heterodimers (Figure 3 and Table 2) provide additional experimental support for a perturbation of the backbone structure. There usually is no energetic penalty for heterodimer formation between a reference gramicidin and analogues with side chain modifications at positions 1 or 2 (*37*). Furthermore, the channels usually show only modest, if any, current−voltage asymmetry (*37*, *41*−*43*), as would be expected if the modifications simply altered the height of the central barrier for ion permeation without introducing strain at the subunit interface. The notable exception is the [F_6Val^1]gA/gA heterodimer that is destabilized relative to both symmetric homodimers (*37*) and for which the current−voltage relation is asymmetric (*44*). [F_6Val^1]gA/gA heterodimers also exhibit voltage-dependent transitions between two conductance states (*40*, *44*). Side chain modifications in the CO-ethanolamide-terminal half of the molecule, toward the channel entrance, usually express themselves in asymmetric current−voltage relations (*39*, *45*−*47*), as would be expected if the modification altered the height of the barrier for ion entry/exit. These channels also have asymmetric lifetime-voltage relations (*39*, *46*). The pronounced asymmetry in the single-channel current amplitudes in Figure 3 thus suggests that the NH → O substitution-induced perturbation propagates away from the channel center, which in turn would establish the observed asymmetry in channel appearances and lifetime. The MD

simulations do, indeed, provide some support for such propagated perturbations in backbone structure.

The bistable behavior of the heterodimeric channels, in which one subunit has a backbone ester, parallels the behavior of other gA heterodimeric channels that are destabilized relative to their parent channels (*38*, *40*). Following this pattern, the [Val-O-Gly]gA/*endo*-Ala^{0a}-D-Ala^{0b}-gA channels have multiple conductance levels, and the probabilities of being in the different conducting states vary as a function of the applied potential (Figure 3). Different charge distributions in an ester as opposed to a peptide bond will give rise to an asymmetry in the backbone dipole; this may contribute to the different patterns of channel appearances at positive and negative potentials (Figure 3).

Channel Activity of the Shortened Hydrolysis Product. As a side product from the spontaneous hydrolysis of the ester bond in [Val-O-Gly]gA, the shorter alcohol [HO-Gly]gA was obtained. The relative lability of the [Val-O-Gly]gA ester bond stands in contrast to the stability of several other ester-substituted proteins: Lu et al. (*5*) reported that although their ester-containing ovomucoid domain had a half-life of only about 4 h at pH 8.7, it was very stable in aqueous buffer up to pH 7.5; similarly, Koh et al. (*3*) reported no degradation of several ester-containing variants of T4 lysozyme during in vitro protein synthesis, purification, reversible thermal denaturation from 20 to 65 °C, and SDS−acrylamide electrophoresis. The T4 lysozyme esters were broken only when deliberately hydrolyzed in concentrated ammonium hydroxide/SDS at 90 °C. In contrast, we have been able to maintain [Val-O-Gly]gA only when it is attached to the resin (stable for many months at 4 °C) or when stored in methanol/water at −80 °C (also for months). The estimated half-life at room temperature in (unbuffered) methanol/water or with aqueous phospholipids is about 1 day. England et al. (*9*) found that the rate of hydrolysis of ester bonds incorporated into nicotinic acetylcholine receptor varied as a function of the amino acid at the *i*-1 position relative to the ester bond, but that large, hydrophobic residues tended to reduce the hydrolysis rate. Perhaps the absence of a side chain on Gly at position 2 enhances the rate of hydrolysis. In fact, the relative instability of [Val-O-Gly]gA resembles that reported for ester analogues of elastin repeating sequences (*8*), in which the ester analogue of valine (hydroxyisovaleric acid) was inserted between two glycines.

The instability toward hydrolysis is a property of the full-length depsi-gramicidin, [Val-O-Gly]gA. By contrast, the short precursor f-Val-O-Gly has a half-life of about 60 days in methanol solution at room temperature (results not shown). The difficulty in characterizing homodimeric [Val-O-Gly]gA/[Val-O-Gly]gA single channels, nevertheless, is due not to chemical lability but rather to the very short lifetimes of these channels (Figure 2).

Because we were unable to characterize the symmetric [Val-O-Gly]gA channels, it is important to ascertain that the channel activity we observe is not the result of inadvertent contamination by the hydrolysis product. The channel-forming properties of the purified hydrolysis product [HO-Gly]gA and, in particular, the characteristics of the heterodimeric channels formed between [HO-Gly]gA and suitable reference gramicidins therefore were examined. Again, the symmetric [HO-Gly]gA channels were difficult to characterize because of their very short duration, but their properties differ from those of the symmetric [Val-O-Gly]gA channels (Figure 2, Table 2). It thus becomes important that [HO-Gly]gA forms heterodimers with 16- as well as with 17-residue gramicidins and that the properties of the [HO-Gly]gA/*endo*-Ala^{0a}-D-Ala^{0b}-gA heterodimers are quite different from those of the [Val-O-Gly]gA/*endo*-Ala^{0a}-D-Ala^{0b}-gA heterodimers. We conclude that we have identified correctly the [Val-O-Gly]gA/*endo*-Ala^{0a}-D-Ala^{0b}-gA heterodimeric channels.

The average lifetimes of the [HO-Gly]gA/*endo*-Ala^{0a}-D-Ala^{0b}-gA and [HO-Gly]gA/*endo*-D-Ala^{0a}-gA heterodimers differ by an order of magnitude (Figures 5 and 6), with the [HO-Gly]gA/*endo*-D-Ala^{0a}-gA channels having the shorter lifetime. Given the alternating L−D- sequence, one would expect that (at least) one of the two heterodimers should have an instability, a missing residue, at the junction between the two subunits; cf. ref *38*. This missing residue would destabilize the heterodimeric channels 25- to 100-fold (*38*). The smaller lifetime of the [HO-Gly]gA/*endo*-D-Ala^{0a}-gA heterodimers, as compared to the [HO-Gly]gA/*endo*-Ala^{0a}-D-Ala^{0b}-gA heterodimers, shows that the former channels have a more pronounced disruption of the subunit interface, meaning that [HO-Gly]gA behaves as if it has an odd number of residues (13), with the HCO-(NH)-terminus replaced by the more bulky HO-CH_2-CO-(NH)-terminus. The relatively modest destabilization of the [HO-Gly]gA/*endo*-D-Ala^{0a}-gA heterodimers relative to the [HO-Gly]gA/*endo*-Ala^{0a}-D-Ala^{0b}-gA heterodimers could reflect an accommodation, by the -OH moiety of the glycolyl-terminus, of one or more H_2O molecules in the gap in the peptide backbone structure. The water molecule(s) could bridge the discontinuity caused by the mismatch in subunit lengths and stabilize the channels by forming hydrogen bonds with both subunits. In any case, the symmetric behavior of the [HO-Gly]gA/*endo*-Ala^{0a}-D-Ala^{0b}-gA heterodimers shows that the perturbation at the subunit interface has only local effects on the channel structure.

Molecular Dynamics Simulations. The most important result of the MD simulations is that, whereas the energy differences between the different dimers are large (and of the correct sign and magnitude), the differences in backbone structures are not very dramatic. The MD results do not provide an obvious explanation for why the [Val-O-Gly]gA/[Val-O-Gly]gA dimer is so extensively destabilized relative to the gA/gA dimer. In structure−function studies typically, the energetic window is about ±17 kJ/mol because any structural change that involves this energy change would cause a 1000-fold change (up or down) in function (*36*). The chemical modification to ester is of this energetic magnitude (per subunit) and has dramatic effects on channel function and stability. Nevertheless, the ester substitution introduces only subtle changes in channel structure.

Although MD did not show major structural changes, the calculated total conformational energies of the different channels (Table 4) are in reasonable aggreement with the experimentally estimated energies. Small changes in average structure and modest differences in dynamics therefore may lead to dramatic functional effects. The largest contributor to the MD-calculated energy differences is the electrostatic component (Table 4), as would be expected for a repulsive interaction between the introduced ester -O- and the C═O of Val^7 (see Figure 8). But the ester → peptide substitution

also will alter the charge distribution at the C═O of Val^1 (*24*, *25*). It is gratifying that the overall energy difference between the gA/gA and the [Val-O-Gly]gA/[Val-O-Gly]gA dimers is similar to the difference in the electrostatic interaction energy between NH^2 and OC^7 versus O^2 and OC^7 (see Results). This result, however, while reasonable, provides little mechanistic insight into why the dimer dissociation rate constant is so much larger for the [Val-O-Gly]gA/[Val-O-Gly]gA, as compared to the gA/gA, dimer. It is striking, however, that the range of hydrogen bond lengths is greater in [Val-O-Gly]gA/[Val-O-Gly]gA than in gA/gA and that the major changes in length occur some distance away ($NH^6 \cdots OC^{11}$ and $NH^8 \cdots OC^{13}$) from the position of the substitution. Moreover, the distribution of intermolecular hydrogen bond lengths is similar in [Val-O-Gly]gA/[Val-O-Gly]gA and gA/gA (results not shown). We conclude that the strain introduced by the electrostatic repulsion between O^2 and OC^7 exerts its effect through (surprisingly) small changes in dimer structure and dynamics.

Functional Effects of the Ester Bond. A peptide → ester substitution can affect gA channel function in several ways, which can be understood by examining the right-handed $\beta^{6.3}$-helical channel structure (Figure 8). First, the dominating effect is the loss of the *intramolecular* hydrogen bond between the N−H of Gly^2 and the C═O of Val^7, together with the introduction of repulsive interactions between the ester -O- and the C═O of Val^7 (of magnitude estimated above). Second, the partial charge on the ester carbonyl oxygen (of Val^1) will be less than that on a peptide carbonyl oxygen (*24*, *25*), which will cause less favorable solvation of permeating cations (*26*) and will weaken the *intermolecular* hydrogen bond between the Val^1 C═O and the N−H of Val^5 in the other monomer. The less favorable ion solvation will increase the energy barrier for cation movement through the center of the pore (*23*), but it is difficult to escape the conclusion that the changes in conductance and lifetime result primarily from (small) perturbations in backbone structure induced by the NH → O substitution. Specifically, replacing the intramolecular hydrogen bond (from NH of Gly^2 to C═O of Val^7) by repulsive >O···O═C interactions would be expected to stress also the neighboring (intramolecular) hydrogen bonds that link the formyl and Gly^2 C═O's to the NHs of Val^7 and Trp^9, respectively, in the next helical turn. The MD simulations provide some support for such propagated perturbations, but they do not help us understand why the peptide → ester substitution has such a large effect on the dissociation rate constant. The first three hydrogen bonds that define the (monomer) folding at the formyl-NH-terminus must somehow be perturbed, which will affect the dynamic and equilibrium behavior of the backbone and, in turn, dimer assembly and stability as well as ion solvation. Yet although they are of significant energy (~29 kJ/mol per subunit), the ester-induced changes in average channel conformation, as calculated by MD, are too small or subtle to provide immediate insights.

The reduction in cation permeability (single-channel conductance) is consistent with the notion that ester carbonyls do not solvate cations as well as peptide carbonyl oxygens (cf. ref *23*), but that cannot be the sole explanation. P_{Cs}/P_{Na}, P_K/P_{Na}, and P_{Cs}/P_K all are decreased, whereas increases would have been expected from a reduction in the effective charge on the carbonyl oxygen (*23*). The observation that both P_{Cs}/P_{Na} and P_{Cs}/P_K are reduced from about 3.0 (for native gA) to less than 1.0 (for dimeric [Val-O-Gly]gA) supports the notion that the peptide → ester substitution somehow perturbs the pore wall. A local, mechanical reduction in the pore radius would more seriously impair the mobility of the larger Cs^+ ion, radius (r) = 1.63 Å, as compared to K^+ (r = 1.33 Å) or Na^+ (r = 0.95 Å).

The *KcsA* potassium channel structure (*15*) shows the importance of the main chain atoms for ion permeation in the narrow ion selectivity filter. The pore-lining Xxx−Gly−Tyr−Gly−Yyy sequence allows for ion solvation by an extended stretch of the peptide backbone, with all of the Xxx, Tyr, and Yyy side chains on the same side of the chain (away from the ion-interaction site). This motif is unique to potassium channels, however, and it is unlikely that the peptide backbone plays a similar critical role in other channels, even though the permeant cation could be solvated by peptide carbonyl oxygens at turns in the structure (e.g., ref *48*). For comparison, the structure of the large conductance, rather nonselective mechanosensitive "MscL" ion channel from *Mycobacterium tuberculosis* (*49*) suggests that backbone atoms are unlikely to be important for solvating the ions that pass through this channel.

Apart from the unique properties conferred by the -Gly−Tyr−Gly- motif in the *KcsA* channel, the important question of whether there is direct backbone involvement with the permeating ions in a particular channel will be determined by the secondary structure of the pore-lining elements. Depending on the packing of these elements, the local structure will give rise to differences in pore size, and thus to different mechanisms underlying the channel's ion activity. It consequently becomes important that the structural and functional roles of the backbone atoms can be examined by introducing ester bonds using genetic methods (*3*, *9*, *50*). Notwithstanding the significance of ion solvation by carbonyl oxygens of the peptide backbone, however, the structural perturbations that are induced by substituting an ester bond for a peptide bond may dominate "simple" changes in solvation energy. In similar fashion, the B24−B25 peptide bond in insulin was replaced by an ester to eliminate an interchain hydrogen bond (*1*), but the major effect was found to be a significant (but local) perturbation of structure, which involved a partial refolding (*2*). Gramicidin channels are similarly affected by a peptide → ester substitution, as the predominant effect is to destabilize the functionally active form. Even when the subunits fold as $\beta^{6.3}$ helices, the changes in channel function are dominated by the replacement of a stabilizing hydrogen bond by a destabilizing O ↔ O contact. More generally, similar structure perturbing effects of peptide → ester substitutions in other channels may impose the dominant effects on channel function.

ACKNOWLEDGMENTS

We thank Christopher Miller for persistent encouragement to introduce an ester bond into the gramicidin channel sequence, Kenneth Turnbull and Matthias McIntosh for invaluable advice on the organic synthesis, James Hinton for help with interpreting and decoupling the NMR spectrum of f-Val-O-Gly, and Marti Scharlau for assistance with the peptide synthesis.

REFERENCES

1. Wollmer, A., Gilge, G., Brandenburg, D., and Gattner, H.-G. (1994) *Biol. **Chem. Hoppe-Seyler 375,** 219−222.*
2. Kurapkat, G., De Wolf, E., Grötzinger, J., and Wollmer, A. (1997) *Protein Sci. 6*, 580−587.
3. Koh, J. T., Cornish, V. W., and Schultz, P. G. (1997) *Biochemistry 36*, 11314−11322.
4. Groeger, C., Wenzel, H. R., and Tschesche, H. (1994) *Int. J. Pept. Protein Res. 44*, 166−172.
5. Lu, W., Qasim, M. A., Laskowski, M., Jr., and Kent, S. B. (1997) *Biochemistry 36*, 673−679.
6. Morgan, B. P., Scholtz, J. M., Ballinger, M. D., Zipkin, I. D., and Bartlett, P. A. (1991) *J. Am. Chem. Soc. 113*, 297−307.
7. Bugg, T. D. H., Wright, G. D., Dutka-Malen, S., Courvalin, P., and Walsh, C. T. (1991) *Biochemistry 30*, 10408−10415.
8. Arad, O., and Goodman, M. (1990) *Biopolymers 29*, 1633−1649.
9. England, P. M., Zhang, Y., Dougherty, D. A., and Lester, H. A. (1999) *Cell 96*, 89−98.
10. Popot, J. L., and Engelman, D. M. (1990) *Biochemistry 29*, 4031−4037.
11. Wimley, W. C., and White, S. H. (1993) *Biochemistry 32*, 6307−6312.
12. White, S. H., and Wimley, W. C. (1999) *Annu. Rev. Biophys. Biomol. Struct. 28*, 319−365.
13. Michel, H., Behr, J., Harrenga, A., and Kannt, A. (1998) *Annu. Rev. Biophys. Biomol. Struct. 27*, 329−356.
14. Cowan, S. W., Schirmer, T., Rummel, G., Steiert, M., and Ghosh, R. (1992) *Nature 358*, 727−733.
15. Doyle, D. A., Cabral, J. M., Pfuetzner, R. A., Kuo, A., Gulbis, J. M., Cohen, S. L., Chait, B. T., and MacKinnon, R. (1998) *Science 280*, 69−77.
16. Andersen, O. S., and Koeppe, R. E., II (1992) *Physiol. Rev. 72*, S89−S158.
17. Hille, B. (1992) *Ionic Channels of Excitable Membranes*, Sinauer Associates, Sunderland, MA.
18. Koeppe, R. E., II, and Andersen, O. S. (1996) *Annu. Rev. Biophys. Biomol. Struct. 25*, 231−258.
19. Urry, D. W. (1971) *Proc. Natl. Acad. Sci. U.S.A. 68*, 672−676.
20. Weinstein, S., Wallace, B. A., Blout, E. R., Morrow, J. S., and Veatch, W. R. (1979) *Proc. Natl. Acad. Sci. U.S.A. 76*, 4230−4234.
21. Arseniev, A. S., Lomize, A. L., Barsukov, I. L., and Bystrov, V. F. (1986) *Biol. Membr. 3*, 1077−1104.
22. Ketchem, R. R., Hu, W., and Cross, T. A. (1993) *Science 261*, 1457−1460.
23. Krasne, S., and Eisenman, G. (1973) *Membranes, Vol. 2: Lipid Bilayers and Antibiotics* (Eisenman, G., Ed.) pp 277−328, Marcel Dekker, New York.
24. Sreerama, N., and Vishveshwara, S. (1985) *Proc. Int. Symp. Biomol. Struct. Interactions, Suppl. J. Biosci. 8*, 315−327.
25. Kallies, B., and Mitzner, R. (1996) *J. Chem. Soc., Perkin Trans. 2*, 1403−1408.
26. Perricaudet, M., and Pullman, A. (1973) *FEBS Lett. 34*, 222−226.
27. Ono, N., Yamada, T., Saito, T., Tanaka, K., and Kaji, A. (1978) *Bull. Chem. Soc. Jpn. 51*, 2401−2404.
28. Greathouse, D. V., Koeppe, R. E., II, Providence, L. L., Shobana, S., and Andersen, O. S. (1999) *Methods Enzymol. 294*, 525−550.
29. Providence, L. L., Andersen, O. S., Greathouse, D. V., Koeppe, R. E., II, and Bittman, R. (1995) *Biochemistry 34*, 16404−16411.
30. Brooks, B. R., Bruccoleri, R. E., Olafson, B. D., States, D. J., Swaminathan, S., and Karplus, M. (1983) *J. Comput. Chem. 4*, 187−217.
31. MacKerell, A. D., Jr., Bashford, D., Bellott, M., Dunbrack, R. L., Jr., Evanseck, J. D., Field, M. J., Fischer, S., Gao, J., Guo, H., Ha, S., Joseph-McCarthy, D., Kuchnir, L., Kuckzera, K., Lau, F. T. K., Mattos, C., Michnick, S., Ngo, T., Nguyen, D. T., Prodhom, B., Reiher, W. E. I., Roux, B., Schlenkrich, M., Smith, J. C., Stote, R., Straub, J., Watanabe, M., Workiewicz-Kuczera, J., Yinb, D., and Karplus, M. (1998) *J. Phys. Chem. B 102*, 3586−3616.
32. Jorgensen, W. L., Chandrasekhar, J., Madura, J. D., Impey, R. W., and Klein, M. L. (1983) *J. Chem. Phys. 79*, 926−935.
33. Regis, P., and Roux, B. (1996) *Biophys. J. 71*, 19−39.
34. Ryckaert, J. P., Cicotti, G., and Berendsen, H. J. C. (1977) *J. Comput. Phys. 23*, 327−341.
35. O'Connell, A. M., Koeppe, R. E., II, and Andersen, O. S. (1990) *Science 250*, 1256−1259.
36. Durkin, J. T., Providence, L. L., Koeppe, R. E., II, and Andersen, O. S. (1992) *Biophys. J. 62*, 145−159.
37. Durkin, J. T., Koeppe, R. E., II, and Andersen, O. S. (1990) *J. Mol. Biol. 211*, 221−234.
38. Durkin, J. T., Providence, L. L., Koeppe, R. E., II, and Andersen, O. S. (1993) *J. Mol. Biol. 231*, 1102−1121.
39. Koeppe, R. E., II, Providence, L. L., Greathouse, D. V., Heitz, F., Trudelle, Y., Purdie, N., and Andersen, O. S. (1992) *Proteins 12*, 49−62.
40. Oiki, S., Koeppe, R. E., II, and Andersen, O. S. (1995) *Proc. Natl. Acad. Sci. U.S.A. 92*, 2121−2125.
41. Mazet, J. L., Andersen, O. S., and Koeppe, R. E., II (1984) *Biophys. J. 45*, 263−276.
42. Russell, E. W. B., Weiss, L. B., Navetta, F. I., Koeppe, R. E., II, and Andersen, O. S. (1986) *Biophys. J. 49*, 673−686.
43. Mattice, G. L., Koeppe, R. E., II, Providence, L. L., and Andersen, O. S. (1995) *Biochemistry 34*, 6827−6837.
44. Oiki, S., Koeppe, R. E., II, and Andersen, O. S. (1994) *Biophys. J. 66*, 1823−1832.
45. Becker, M. D., Greathouse, D. V., Koeppe, R. E., II, and Andersen, O. S. (1991) *Biochemistry 30*, 8830−8839.
46. Fonseca, V., Daumas, P., Ranjalahy Rasoloarijao, L., Heitz, F., Lazaro, R., Trudelle, Y., and Andersen, O. S. (1992) *Biochemistry 31*, 5340−5350.
47. Jude, A. R., Greathouse, D. V., Koeppe, R. E., II, Providence, L. L., and Andersen, O. S. (1999) *Biochemistry 38*, 1030−1039.
48. Lipkind, G. M., and Fozzard, H. A. (1994) *Biophys. J. 66*, 1−13.
49. Chang, G., Spencer, R. H., Lee, A. T., Barclay, M. T., and Rees, D. C. (1998) *Science 282*, 2220−2226.
50. Ellman, J. A., Mendel, D., and Schultz, P. G. (1992) *Science 255*, 197−200.
51. Killian, J. A., Taylor, M. J., and Koeppe, R. E., II (1992) *Biochemistry 31*, 11283−11290.

BI001562Y